

**Mimicing the Kane-Mele type spin orbit interaction by spin-flexual phonon
coupling in graphene devices**

Jianlei Ge^{1,†}, Rui Wang^{1,†}, Tianru Wu^{2,†}, Jing Li³, Yuyuan Qin¹, Fucong Fei¹, Shuai Zhang¹, Zhanbin Bai¹, Liling Sun⁴, Lu Cao¹, Xuefeng Wang⁵, Xinran Wang⁵, Fengqi Song^{1,*}, You Song^{3,*}, Baigeng Wang^{1,*}, Guanghou Wang¹

¹National Laboratory of Solid State Microstructures, College of Physics and Collaborative Innovation Center of Advanced Microstructures, Nanjing University, Nanjing 210093, China

²State Key Laboratory of Functional Materials for Informatics, Shanghai Institute of Microsystem and Information Technology, Chinese Academy of Sciences, Shanghai 200050, China

³Collaborative Innovation Center of Advanced Microstructures, State Key Laboratory of Coordination Chemistry, and School of Chemistry and Chemical Engineering, Nanjing University, Nanjing 210023, China

⁴Institute of Physics, Beijing National Laboratory for Condensed Matter Physics and Collaborative Innovation Center of Quantum Matter, Chinese Academy of Sciences, Beijing 100190, China

⁵National Laboratory of Solid State Microstructures, Collaborative Innovation Center of Advanced Microstructures, and School of Electronic Science and Engineering, Nanjing University, Nanjing 210093, China

[†] J.Ge, R.Wang and T.Wu contributed equally to this work.

* Corresponding authors. F.S. (songfengqi@nju.edu.cn), Y.S. (yousong@nju.edu.cn), B.W. (bgwang@nju.edu.cn). Fax: +86-25-83595535

Abstract:

On the efforts of enhancing the spin orbit interaction (SOI) of graphene for seeking the dissipationless quantum spin Hall devices, unique Kane-Mele type SOI and high mobility samples are desired. However, common external decoration often introduces extrinsic Rashba-type SOI and simultaneous impurity scattering. Here we show, by the EDTA-Dy molecule dressing, the Kane-Mele type SOI is mimicked with even improved carrier mobility. It is evidenced by the suppressed weak localization at equal carrier densities and simultaneous Elliot-Yafet spin relaxation. The extracted spin scattering time is monotonically dependent on the carrier elastic scattering time, where the Elliot-Yafet plot gives the interaction strength of 3.3 meV. Improved quantum Hall plateaus can be even seen after the external operation. This is attributed to the spin-flexural phonon coupling induced by the enhanced graphene ripples, as revealed by the in-plane magnetotransport measurement.

Key words:

graphene; ripple; spin-orbit interaction; flexural phonon; weak localization

Intense efforts have been made on enhancing the spin orbit interaction (SOI) of graphene because of the potential quantum spin hall (QSH) effect^{1, 2, 3, 4, 5, 6, 7, 8, 9, 10, 11, 12, 13, 14, 15, 16}, which was firstly proposed on graphene and recently demonstrated in HgTe/CdTe quantum wells^{5, 8}, InAs/GaSb,^{11, 13} single-layer FeSe¹⁵ and monolayer WTe₂ systems¹⁶. The critical obstacle for the graphene's QSH is that the chemical potential has to be tuned into the SOI-generated gap of the Dirac cone. However, the SOI gap is very small for pristine graphene, i.e. $\sim 10^{-5} \sim 10^{-6}$ eV^{17, 18}. The SOI-enhancing proposals include functionalizing the graphene with some light atoms, e.g. hydrogenated graphene^{19, 20} and fluorinated graphene²¹, decorating the graphene with metallic atoms, such as In²², Au^{23, 24}, and attaching graphene to strong spin-orbit coupling materials, such as Bi₂Te₂Se²⁵, Bi₂Se₃²⁶ and have been implemented with the improved SOI of $\sim 10^{-2}$ eV^{9, 19, 21, 22, 23, 24, 25, 26, 27, 28, 29}.

However, in order to achieve the QSH, the SOI type has to be the Kane-Mele (KM) desired type with the Hamiltonian of $\sim \tau_z \sigma_z s_z$, because the common Rashba SOI ($\sim \vec{z} \cdot (\vec{s} \times \vec{\sigma})$) may break the QSH transport by mixing different branches of spin channels¹⁷. This is reasonable since the KM type SOI is originated from the symmetry of the graphene honeycomb lattice. Furthermore, the above external decoration may simultaneously suppress the mobility of graphene and subsequently destroys rather fragile QSH edge states.

Here we show that the KM type SOI can be mimicked by a spin-flexural phonon coupling picture, which is implemented by dressing the graphene devices using Na[Dy(EDTA)(H₂O)₃] \cdot 5H₂O (EDTA-Dy) molecules. The Elliot-Yafet (EY) plot of

spin scattering time and carrier elastic scattering time gives the SOI strength of 3.3 meV. The graphene devices even present improved half-integer quantum Hall transport after externally dressed.

Improved transport after the external dressing of EDTA-Dy

The graphene device was fabricated on a single crystal grain of chemical vapor deposition grown graphene sheet (**Figure 1(a)**). The EDTA-Dy is a kind of stable and aqueous soluble dysprosium complex molecule. Fig. 1(b) shows its infrared spectrum, where the characteristic peaks positioned at 3430, 1610, 1380 and 1100 cm^{-1} are respectively the stretching vibration mode of O-H in coordinated water molecules or free water molecules, C=O in EDTA ligand, C-O in the carboxyl of EDTA ligand and N-C in EDTA ligand. This points to the characteristic coordinated anion $[\text{Dy}(\text{EDTA})(\text{H}_2\text{O})_3]^-$, a cation Na^+ and five lattice water molecules as shown in the inset of Fig. 1(b). Fig. 1(c) shows the Raman spectrum of EDTA-Dy dressed graphene, where the 2D/G peak ratio is 1.44 and the full width half maximum (FWHM) of the 2D peak is 25.01 cm^{-1} . These confirm the monolayer thickness of the graphene sheet. Transport parameters of the four measured devices are listed in Table I.

Fig. 1(d) shows the relationship between the longitudinal resistance (R_{xx}) and back gate voltage (V_g) of EDTA-Dy dressed graphene at 2, 20 and 290 K, where the device's bipolar behavior is obvious. We find that after EDTA-Dy dressing, the density of hole carriers decreases. This means the electronic transfer from the EDTA-Dy molecules to graphene, which can be understood through the structure of

EDTA-Dy. The EDTA ligand in EDTA-Dy complex has four $-\text{COO}^-$ groups which chelate with one Dy^{III} ion. The $-\text{COO}^-$ group has free O^{2-} with large electron density. The O^{2-} in $-\text{COO}^-$ group has a strong tendency to interact with the π electrons of the benzene ring of the graphene.

Interestingly, the performances of the graphene devices are improved after the dressing using the EDTA-Dy coating as also seen in graphene grafted with Pt-porphyrins.³⁰ The carrier mobility unexpectedly changes from 1919 to 3226 $\text{cm}^2\text{V}^{-1}\text{s}^{-1}$ after the external coating. One can see quantum Hall effect (QHE) in the devices as shown in Fig. 1(e). The V_g dependence of the longitudinal resistivity ρ_{xx} and the hall conductivity σ_{xy} were measured in a magnetic field of 12 T at a temperature of 2 K. The Hall conductivity goes quantized when the longitudinal resistivity approaches zero. The plateau series of $4n+2$ is the characteristic half-integer QHE of monolayer graphene.^{31, 32} The zero-filling plateau is clear, showing satisfactory electrical transport of the devices.

Suppressed WL and selectively-enhanced KM-type SOI

The electronic SOI alters the interference in a pair of time-reversal loops, which causes the phase shift and quantum modification to the low-field MR curves.^{33, 34} For graphene, E. McCann's weak localization (WL) theory describes the low-field WL correction with a KM-type SOI to the conductivity as below^{35, 36}

$$\Delta\sigma(B) = -\frac{e^2}{2\pi h} \left[-2F\left(\frac{B}{B_\varphi + B_{KM}}\right) + 4F\left(\frac{B}{B_\varphi + B_* + B_{KM}}\right) + 2F\left(\frac{B}{B_\varphi + 2B_i + B_{KM}}\right) \right], \quad (1)$$

$$F(z) = \ln z + \psi\left(\frac{1}{2} + \frac{1}{z}\right), B_{\varphi,i,*,KM} = \frac{\hbar c}{4De} \tau_{\varphi,i,*,KM}^{-1},$$

where ψ is the digamma function, D is the diffusion coefficient, τ_φ^{-1} is the inelastic dephasing rate, τ_*^{-1} is the intravalley symmetry-breaking scattering rate, τ_i^{-1} is the intervalley scattering rate, and τ_{KM}^{-1} is the intrinsic KM spin relaxation rate. The relaxation length scales are related to the relaxation times as $L_{\varphi,i,*} = \sqrt{D\tau_{\varphi,i,*}}$. E. McCann *et al* further predicts that the type of SOI can be identified by analyzing the WL features and spin relaxation mechanism.^{35,37} When intense SOI is introduced into graphene, weak antilocalization and D'yakonov-Perel (DP) spin relaxation suggest the dominance of the Rashba-type SOI, while the suppressed WL and EY spin relaxation indicate the dominance of KM type SOI.

The low-field magnetoconductance of the graphene before and after the EDTA-Dy dressing is shown in Fig. 2(a) and (b) respectively. The device's conductance is sharply suppressed at zero fields, and its amplitudes decrease with the increasing temperature, which is attributed to the WL effect. By tuning V_g , we obtain the same charge density of $5.3 \times 10^{12} \text{ cm}^{-2}$ for the devices both before and after the dressing for the same devices. This allows us to compare the SOI strength at the same Fermi level. The WL feature of the EDTA-Dy dressed graphene is only around a quarter of that of the pristine graphene. This reveals the suppressed WL, agreeing with the KM SOI dominant case in E. McCann's WL theory³⁵.

The WL features can be tuned by V_g . Applying the gate voltage from -30V to 90V, we can find that the amplitudes and shapes of the WL features are changed systematically as shown in Fig. 2(c). Fitting all the WL data with Eq. (1), we can extract the transport parameters including the spin scattering time τ_{KM} . The typical electronic dephasing length L_φ , intervalley scattering length L_i and intravalley scattering length L_* are 650, 60 and 20 nm respectively. In Fig. 2(d), we plot the extracted values of τ_{KM} against V_g at different temperatures, where we can see τ_{KM} increases while V_g is away from the charge neutral point ($V_{\text{Dirac}} \approx 62$ V). It increases to over 400 ps by two orders at the negative gate voltages. This demonstrates the convenient spin transport control in EDTA-Dy dressed graphene.

Further discussions reveal the spin relaxation mechanism in the devices. The DP procedure occurs through spin precessions while the EY procedure develops through the spin flips by the scatterers. They cause distinct dependence of spin relaxation time on the elastic scattering time τ_p , where $\tau_p = h\sigma / (2e^2 v_F \sqrt{\pi n})$. With the measurement of conductivity and carrier density at each V_g , we can obtain the values of τ_p . We find that τ_{KM} is monotonically increasing with τ_p as shown in Fig. 2(e), which is the signature of the EY spin relaxation. We make the EY plot $\tau_{KM} = \tau_p (\varepsilon_F / \Delta_{KM})^2$ in Fig. 2(e), where Δ_{KM} is the strength parameter of the SOI causing the spin relaxation and ε_F is the chemical potential as compared to the Dirac point. Nice fittings are seen at all temperatures, indicating the dominance of the EY relaxation. Thus we obtain the effective SOI strength of the EDTA-Dy dressed graphene devices.

We find that the SOI strength increases with the rising temperature both in pristine and dressed graphene as shown in Fig. 2(e). It is believed that the SOI (Δ_{D0}) which generates the Dirac cone gap will not change with the temperature. We therefore extrapolate the data along the linear fitting and expect Δ_{D0} by checking the intercepts at zero temperature. It is found that Δ_{D0} is quite small for pristine graphene, while it achieves 3.3meV after the EDTA-Dy dressing. Such Δ_{D0} has been large enough to accommodate the QSH states in the devices. The temperature-dependent SOI is attributed to the electronic scattering by the impurity centers.^{38, 39}

Dressing induced ripples revealed by in-plane magnetic field

As stated above, both the suppressed WL and successful EY plot reveal the selectively enhanced KM-type SOI while dressing the graphene sheet using EDTA-Dy molecules. Such external dressing should induce more scattering, but the present devices even show improved quantum transport, whose physics forms the main question of this work. We propose the ripples caused by the stretching EDTA-Dy coating might contribute the pseudo magnetic field (gauge field), which prefers the KM-type SOI in graphene.

Such ripples are revealed by the atomic force microscopy (AFM) measurement as shown in Fig. 3(a). The root-mean-square (RMS) roughness of pristine graphene is 0.66 nm. After EDTA-Dy dressing, the RMS height of graphene increases to 1.64 nm. Similar ripples have been described in PTSA coated graphene⁴⁰. This can be understood by the interfacial stretching due to the different temperature-dependent

shrinking of graphene and the organic film. Such ripples even detach some part of graphene from the substrates and suppress the charge scattering from the substrates^{41,}

⁴².

To obtain the in-situ RMS information of the dressed graphene⁴³, we measure the MR curves of the device under in-plane fields. As proposed by J. A. Folk *et al*, the ripple configuration in graphene can be measured by applying an in-plane magnetic field, when a random vector potential (RVP) field is generated and modifies the MR response.⁴⁴ The RVP-modified magnetoresistivity $\Delta\rho(B_{\parallel})$ for Gaussian ripples can be calculated by a Boltzmann approach⁴⁴:

$$\Delta\rho(n, \theta, B_{\parallel}) = \frac{\sin^2\theta + 3\cos^2\theta}{4} \frac{1}{\hbar|n|^{3/2}} \frac{Z^2}{R} B_{\parallel}^2, \quad (2)$$

where θ is the angle between the current flow and B_{\parallel} , as shown in the inset of Fig. 3(b). Z is RMS height and R is correlation length. The graphene before and after the EDTA-Dy dressing is measured with $\theta \approx 10^\circ$ and 80° , which gives $Z^2/R \approx 0.14 \text{ nm}$ and 0.67 nm respectively by fitting Eq. (2).

Further measurements have to be carried out to obtain the RMS (Z). Parallel-field-generated magnetic flux through the ripples causes orbital effects, due to which the phase-coherent WL can be suppressed. For this, we design the experiment to measure the WL features driven by a perpendicular field while applying a series of fixed parallel fields.

As known, the WL features driven by a perpendicular field can be formulated as below⁴⁵

$$\Delta\sigma(B_{\perp}) = \frac{e^2}{\pi h} \left[F\left(\frac{\tau_B^{-1}}{\tau_{\phi}^{-1}}\right) - F\left(\frac{\tau_B^{-1}}{\tau_{\phi}^{-1} + 2\tau_i^{-1}}\right) - 2F\left(\frac{\tau_B^{-1}}{\tau_{\phi}^{-1} + \tau_i^{-1} + \tau_*^{-1}}\right) \right], \quad (3)$$

where $\tau_B^{-1} = 4eDB_{\perp}/\hbar c$. In Fig. 3(c) the WL is very obvious and the WL scattering rates are extracted from measured curves by fitting to Eq. (3), in which $\tau_{\varphi}^{-1}, \tau_i^{-1}$ and τ_*^{-1} are 1.14×10^{11} , 6.01×10^{10} and $1.18 \times 10^{14} \text{ s}^{-1}$ respectively for the $B_{\parallel} = 0$ case.

The WL dip is further suppressed after applying an in-plane field as shown in Fig. 3(c) and (d), where Eq. (3) is fitted in multiple magnetoconductivity curves with a series of B_{\parallel} . During the fitting, τ_i^{-1} and τ_*^{-1} are fixed. Extracted values of τ_{φ}^{-1} plotted against B_{\parallel}^2 are shown in Fig. 3(e), and linear fit confirms the dependence in Eq. (4) proposed by J. A. Folk *et al*⁴⁴, with $Z^2R = 1.07 \text{ nm}^3$.

$$\tau_{\varphi}^{-1} \rightarrow \tau_{\varphi}^{-1} + \sqrt{\pi}(e^2/\hbar^2)vZ^2RB_{\parallel}^2 \quad (4)$$

By using the values of Z^2/R and Z^2R , $Z = 0.62 \text{ nm}$ and $R = 2.7 \text{ nm}$ are obtained for Gaussian-correlated ripples for the pristine graphene. Similarly, $Z = 1.48 \text{ nm}$ and $R = 3.2 \text{ nm}$ are the ripple dimensions of EDTA-Dy dressed graphene. This confirms the ripple generation by the EDTA-Dy coating.

Spin-flexural phonon coupling mode in rippled graphene

Here we propose that the EY spin relaxation can be interpreted by the flexural phonon mode in rippled graphene. This is partially based on the previous study on all symmetry-adapted spin-phonon couplings⁴⁶, where the phonons vibration associated to the B_2 irreducible representation generates a correction term to the electrons, $H_{ph} = g\sigma^z s^z h(\mathbf{r})^2$, where $h(\mathbf{r})$ is the vertical displacement of the atoms, σ and s are Pauli matrices defined in the sublattice and spin, respectively. Considering the

thermal average, the phonon mode further results in a local term that reads as $H_{KM} = \Delta(\mathbf{r})\sigma^z s^z$. $\Delta(\mathbf{r})$ is proportional to $\langle h^2 \rangle$. The low-energy effective model reads as,

$$H_{eff} = -i\hbar v_F \boldsymbol{\sigma} \cdot \nabla + \Delta(r)\sigma^z s^z. \quad (5)$$

This effective Hamiltonian becomes a KM-like term and explains the dominance of the KM-type SOI in our study.

This model reasonably predicts that only the in-plane spins would undergo the spin-flip during scattering since the z component of spins are conserved. $\Delta(r)$ can be treated as disorder characterized by the Gaussian type delta function-correlated function, i.e., $\langle \Delta(r) \rangle = 0$ and $\langle \Delta(r)\Delta(r') \rangle = \bar{\Delta}\delta(r - r')$. Then dealing with the disorder average^{47, 48, 49} (see supplementary), it can be shown that a global effective KM-like term would take place in mean-field level. Solving the corresponding Schrodinger equation, one can obtain the spin-flip probability which reads as $\alpha = \frac{\bar{\Delta}^2}{4\varepsilon_F^2}$. This finally lead to a EY type spin relaxation time that satisfy $\tau_s = \varepsilon_F^2 \tau_p / \bar{\Delta}^2$, accounting for the experimental results in Fig.2.

To further study the temperature dependence of the spin lifetime, we resort to a second quantization form of the phonon field. In this form, the spin-phonon interaction is reduced to

$$H_{ph} = \sum_{\mathbf{k}, \mathbf{q}, \mathbf{q}'} V_{\mathbf{k}, \mathbf{q}, \mathbf{q}'} \mathcal{C}_{\mathbf{k}+\mathbf{q}+\mathbf{q}'}^+ \sigma_z s_z \mathcal{C}_{\mathbf{k}} (d_{\mathbf{q}} + d_{-\mathbf{q}}^+) (d_{\mathbf{q}'} + d_{-\mathbf{q}'}^+) \quad (6)$$

where $V_{\mathbf{k}, \mathbf{q}, \mathbf{q}'} = \frac{g\hbar}{2\rho \sqrt{\omega_{\mathbf{q}}\omega_{\mathbf{q}'}}}$, $\omega_{\mathbf{q}}$ is the phonon dispersion, ρ is the mass density of the

Carbon atoms, and $\mathcal{C}_{\mathbf{k}}$ is a four-dimensional electron spinor in sublattice and spin space. Evaluating the spin-flip scattering probability and using the Fermi's golden

sum rule, the spin relaxation rate can be obtained. For higher temperature region with $T > \hbar\omega_F/k_B$, which is the experimental case⁵⁰, we arrive at,

$$\frac{1}{\tau_s} = AT^2 + BT + C \quad (7)$$

where A and B are the second order and first order T-dependence coefficient respectively, while C is a constant representing the zero temperature residue contribution⁴⁶. As an estimation, neglecting the dispersion of phonon and replacing the integral by an averaged frequency $\bar{\omega}$, then A and B can be found to satisfy $A = \frac{64g^2k_B^2k_F^3}{\pi\hbar^2v_F\rho^2\bar{\omega}^4}$ and $B = \frac{64g^2k_Bk_F^3}{\pi\hbar v_F\rho^2\bar{\omega}^3}$. For experimental values, we take $\rho = 7.6 \times 10^{-7} \text{ kg} \cdot \text{m}^{-2}$ and $\bar{\omega} = 10 \text{ meV}$. In addition, g is related to the strength of KM-like SOC. From the inset of Fig.2e, g can be set to be $g \simeq 2 \text{ eV} \cdot \text{\AA}^{-2}$. Then, the parameter A and B can be estimated to be $A \simeq 2.0 \times 10^{-6} \text{ K}^{-2}\text{ps}^{-1}$ and $B \simeq 2.3 \times 10^{-4} \text{ K}^{-1}\text{ps}^{-1}$, respectively.

In Fig.4, we fit the experimental $\frac{1}{\tau_s} - T$ curve according to Eq.(7), the fitted parameters of the first graphene device after EDTA-Dy dressing are found to be $A = 1.9 \times 10^{-6} \text{ K}^{-2}\text{ps}^{-1}$ and $B \simeq 1.86 \times 10^{-4} \text{ K}^{-1}\text{ps}^{-1}$, in well agreement with our estimated values. As can be seen from Fig.4, while it is almost negligible in the pristine sample, an obvious temperature dependence of the spin life time is found to emerge in the dressed graphene.

Conclusion

We can selectively enhance the KM-type SOI in graphene by using the EDTA-Dy dressing, as evidenced by the suppressed WL and simultaneous EY spin relaxation.

The SOI strength of 3.3 meV is achieved. The Quantum Hall effect can be seen with a $4n+2$ series of plateaus even after the external dressing. We believe the interfacial stretching and local ripple configuration may achieve the simultaneous external SOI control and transport improvement. A spin-flexural phonon coupling model is proposed. Such subtle control of the electronic properties paves the way towards the topological insulator states in graphene.

Methods

The graphene devices were fabricated on a single crystal grain of chemical vapor deposition grown graphene sheet, which were selected by optical microscopy and transferred to the Si substrate with a 300-nm-thick SiO₂ layer. Standard e-beam lithography and metallization processes were used to make the Hall bar structures. Electrodes are made of 5-nm-thick Ti and 35-nm-thick Au by the e-beam evaporation.

The EDTA-Dy complex is prepared according the improved methods reported in Ref⁵¹. 10 mL aqueous solution of EDTANa₂ (7.44 g, 0.02 mol) was added into 10 mL aqueous solution of Dy(NO₃)₃ • 5H₂O (8.77 g, 0.02 mol) with stirring and the pH value was adjusted to 6.5 by 1 M NaOH aqueous solution. When the precipitation was observed, the additional water was added to 200 mL of the solution. Overnight, crystalline product as colorless block of EDTA-Dy appeared.

The influence of EDTA-Dy coating on graphene was investigated by Raman spectroscopy, AFM and electrical transport measurements. Raman spectra were measured at room temperature with a Renishaw spectrometer over wave numbers

from 1000 to 3000 cm^{-1} with the laser wavelength of 633 nm. The surface morphology of the CVD grown graphene was characterized by AFM (Asylum Research Cypher S). Electrical transport measurements were done in Cryomagnetics' C-Mag system by a standard low-frequency lock-in technique. Pristine graphene was measured in the system and then it was processed by a little drop of EDTA-Dy solution. The processed graphene was kept in fuming cupboard for minutes to dry off. EDTA-Dy decorated graphene was then recooled and measured in the system. A vector magnet is used in in-plane field measurements. The charge density is obtained through Hall measurements according to the relation $n = 1/qR_H$, where q is the electronic charge and R_H is the hall coefficient obtained by fitting $R_{xy} \sim B(T)$ with the linear curve at low magnetic field (± 1 T). The carrier mobility can be obtained using the relation $\mu = \sigma/nq$ where σ is the conductivity. The mean free path and diffusion coefficient of carrier also can be obtained from $l_e = h\sigma/(2q^2\sqrt{\pi n})$ and $D = v_F l_e/2$, where the fermi velocity $v_F \approx 10^6$ m/s.

References

1. Kane CL, Mele EJ. Z_2 Topological Order and the Quantum Spin Hall Effect. *Phys Rev Lett* 2005, **95**(14): 146802.
2. Kane CL, Mele EJ. Quantum Spin Hall Effect in Graphene. *Phys Rev Lett* 2005, **95**(22): 226801.
3. Bernevig BA, Hughes TL, Zhang S-C. Quantum Spin Hall Effect and Topological Phase Transition in HgTe Quantum Wells. *Science* 2006, **314**(5806): 1757-1761.
4. Bernevig BA, Zhang S-C. Quantum Spin Hall Effect. *Phys Rev Lett* 2006, **96**(10): 106802.
5. König M, Wiedmann S, Brüne C, Roth A, Buhmann H, Molenkamp LW, *et al.* Quantum Spin Hall Insulator State in HgTe Quantum Wells. *Science* 2007, **318**(5851): 766-770.
6. Shuichi M. Phase transition between the quantum spin Hall and insulator phases in 3D: emergence of a topological gapless phase. *New Journal of Physics* 2007, **9**(9): 356.
7. Roy R. Topological phases and the quantum spin Hall effect in three dimensions. *Phys Rev B* 2009, **79**(19): 195322.
8. Roth A, Brüne C, Buhmann H, Molenkamp LW, Maciejko J, Qi X-L, *et al.* Nonlocal Transport in the Quantum Spin Hall State. *Science* 2009, **325**(5938): 294-297.
9. Weeks C, Hu J, Alicea J, Franz M, Wu R. Engineering a Robust Quantum Spin Hall State in Graphene via Adatom Deposition. *Phys Rev X* 2011, **1**(2): 021001.
10. Liu C-C, Feng W, Yao Y. Quantum Spin Hall Effect in Silicene and Two-Dimensional Germanium. *Phys Rev Lett* 2011, **107**(7): 076802.
11. Knez I, Du R-R, Sullivan G. Andreev Reflection of Helical Edge Modes in InAs/GaSb Quantum Spin Hall Insulator. *Phys Rev Lett* 2012, **109**(18): 186603.
12. Xu Y, Yan B, Zhang H-J, Wang J, Xu G, Tang P, *et al.* Large-Gap Quantum Spin Hall Insulators in Tin Films. *Phys Rev Lett* 2013, **111**(13): 136804.
13. Knez I, Rettner CT, Yang S-H, Parkin SSP, Du L, Du R-R, *et al.* Observation of Edge Transport in the Disordered Regime of Topologically Insulating InAs/GaSb Quantum Wells. *Phys Rev Lett* 2014, **112**(2): 026602.

14. Qian X, Liu J, Fu L, Li J. Quantum spin Hall effect in two-dimensional transition metal dichalcogenides. *Science* 2014, **346**(6215): 1344-1347.
15. Wang ZF, Zhang H, Liu D, Liu C, Tang C, Song C, *et al.* Topological edge states in a high-temperature superconductor FeSe/SrTiO₃(001) film. *Nat Mater* 2016, **15**(9): 968-973.
16. Fei Z, Palomaki T, Wu S, Zhao W, Cai X, Sun B, *et al.* Topological insulator behavior in monolayer WTe₂. *arXiv:161007924* 2016.
17. Gmitra M, Konschuh S, Ertler C, Ambrosch-Draxl C, Fabian J. Band-structure topologies of graphene: Spin-orbit coupling effects from first principles. *Phys Rev B* 2009, **80**(23): 235431.
18. Yao Y, Ye F, Qi X-L, Zhang S-C, Fang Z. Spin-orbit gap of graphene: First-principles calculations. *Phys Rev B* 2007, **75**(4): 041401.
19. Balakrishnan J, Kok Wai Koon G, Jaiswal M, Castro Neto AH, Ozyilmaz B. Colossal enhancement of spin-orbit coupling in weakly hydrogenated graphene. *NatPhys* 2013, **9**(5): 284-287.
20. Elias DC, Nair RR, Mohiuddin TMG, Morozov SV, Blake P, Halsall MP, *et al.* Control of Graphene's Properties by Reversible Hydrogenation: Evidence for Graphane. *Science* 2009, **323**(5914): 610-613.
21. Withers F, Dubois M, Savchenko AK. Electron properties of fluorinated single-layer graphene transistors. *Phys Rev B* 2010, **82**(7): 073403.
22. Jia Z, Yan B, Niu J, Han Q, Zhu R, Yu D, *et al.* Transport study of graphene adsorbed with indium adatoms. *Phys Rev B* 2015, **91**(8): 085411.
23. Marchenko D, Varykhalov A, Scholz MR, Bihlmayer G, Rashba EI, Rybkin A, *et al.* Giant Rashba splitting in graphene due to hybridization with gold. *NatComm* 2012, **3**: 1232.
24. Wang Y, Cai X, Reutt-Robey J, Fuhrer MS. Neutral-current Hall effects in disordered graphene. *Phys Rev B* 2015, **92**(16): 161411.
25. Lee P, Jin K-H, Sung SJ, Kim JG, Ryu M-T, Park H-M, *et al.* Proximity Effect Induced Electronic Properties of Graphene on Bi₂Te₂Se. *ACS Nano* 2015, **9**(11): 10861-10866.
26. Rajput S, Li Y-Y, Weinert M, Li L. Indirect Interlayer Bonding in Graphene–Topological Insulator van der Waals Heterostructure: Giant Spin–Orbit Splitting of the Graphene Dirac States. *ACS Nano* 2016, **10**(9): 8450-8456.
27. Zhou J, Liang Q, Dong J. Enhanced spin–orbit coupling in hydrogenated and fluorinated graphene. *Carbon* 2010, **48**(5): 1405-1409.

28. Jiang H, Qiao Z, Liu H, Shi J, Niu Q. Stabilizing Topological Phases in Graphene via Random Adsorption. *Phys Rev Lett* 2012, **109**(11): 116803.
29. Zhang J, Triola C, Rossi E. Proximity Effect in Graphene\char21{ }Topological-Insulator Heterostructures. *Phys Rev Lett* 2014, **112**(9): 096802.
30. Li C, Komatsu K, Bertrand S, Clavé G, Campidelli S, Filoramo A, *et al.* Signature of gate-tunable magnetism in graphene grafted with Pt-porphyrins. *Phys Rev B* 2016, **93**(4): 045403.
31. Novoselov KS, Geim AK, Morozov SV, Jiang D, Katsnelson MI, Grigorieva IV, *et al.* Two-dimensional gas of massless Dirac fermions in graphene. *Nature* 2005, **438**(7065): 197-200.
32. Zhang Y, Tan Y-W, Stormer HL, Kim P. Experimental observation of the quantum Hall effect and Berry's phase in graphene. *Nature* 2005, **438**(7065): 201-204.
33. Bergman G. Influence of Spin-Orbit Coupling on Weak Localization. *Phys Rev Lett* 1982, **48**(15): 1046-1049.
34. Koga T, Nitta J, Akazaki T, Takayanagi H. Rashba Spin-Orbit Coupling Probed by the Weak Antilocalization Analysis in $\text{InAlAs}/\text{InGaAs}/\text{InAlAs}$ Quantum Wells as a Function of Quantum Well Asymmetry. *Phys Rev Lett* 2002, **89**(4): 046801.
35. McCann E, Fal'ko VI. Weak Localization and Spin-Orbit Coupling in Monolayer and Bilayer Graphene. In: Aoki H, S. Dresselhaus M (eds). *Physics of Graphene*. Springer International Publishing: Cham, 2014, pp 327-345.
36. Ge J-L, Wu T-R, Gao M, Bai Z-B, Cao L, Wang X-F, *et al.* Weak localization of bismuth cluster-decorated graphene and its spin-orbit interaction. *Frontiers of Physics* 2017, **12**(4): 127210.
37. McCann E, Fal'ko VI. \rightarrow -z Symmetry of Spin-Orbit Coupling and Weak Localization in Graphene. *Phys Rev Lett* 2012, **108**(16): 166606.
38. Fishman G, Lampel G. Spin relaxation of photoelectrons in p -type gallium arsenide. *Phys Rev B* 1977, **16**(2): 820-831.
39. Ohno Y, Terauchi R, Adachi T, Matsukura F, Ohno H. Spin Relaxation in GaAs(110) Quantum Wells. *Phys Rev Lett* 1999, **83**(20): 4196-4199.
40. Singh AK, Iqbal MW, Singh VK, Iqbal MZ, Lee JH, Chun S-H, *et al.* Molecular n-doping of

- chemical vapor deposition grown graphene. *Journal of Materials Chemistry* 2012, **22**(30): 15168-15174.
41. Ishigami M, Chen JH, Cullen WG, Fuhrer MS, Williams ED. Atomic Structure of Graphene on SiO₂. *Nano Lett* 2007, **7**(6): 1643-1648.
 42. Du X, Skachko I, Barker A, Andrei EY. Approaching ballistic transport in suspended graphene. *Nat Nano* 2008, **3**(8): 491-495.
 43. this avoid the artificial effect while removing the coating layer
 44. Lundeberg MB, Folk JA. Rippled Graphene in an In-Plane Magnetic Field: Effects of a Random Vector Potential. *Phys Rev Lett* 2010, **105**(14): 146804.
 45. McCann E, Kechedzhi K, Fal'ko VI, Suzuura H, Ando T, Altshuler BL. Weak-Localization Magnetoresistance and Valley Symmetry in Graphene. *Phys Rev Lett* 2006, **97**(14): 146805.
 46. Ochoa H, Castro Neto AH, Fal'ko VI, Guinea F. Spin-orbit coupling assisted by flexural phonons in graphene. *Phys Rev B* 2012, **86**(24): 245411.
 47. Pruisken AMM, Schäfer L. Field Theory and the Anderson Model for Disordered Electronic Systems. *Phys Rev Lett* 1981, **46**(7): 490-492.
 48. Pruisken AMM, Schäfer L. The Anderson model for electron localisation non-linear σ model, asymptotic gauge invariance. *Nucl Phys B* 1982, **200**(1): 20-44.
 49. Wegner F. The mobility edge problem: Continuous symmetry and a conjecture. *Zeitschrift für Physik B Condensed Matter* 1979, **35**(3): 207-210.
 50. Vicent I, Ochoa H, Guinea F. Spin relaxation in corrugated graphene. *arXiv preprint arXiv:170205820* 2017.
 51. Nassimbeni LR, Wright MRW, van Niekerk JC, McCallum PA. Packing patterns in lanthanide-edta complexes: crystal and molecular structures of sodium triqua(ethylenediaminetetraacetato)dysprosate(III) pentahydrate and caesium diaqua(ethylenediaminetetraacetato)ytterbate(III) trihydrate. *Acta Crystallographica Section B* 1979, **35**(6): 1341-1345.

Acknowledgments

We thank Yongchun Tao for helpful discussions. We gratefully acknowledge the financial support of the National Key Projects for Basic Research of China (Grant Nos: 2013CB922100), the National Natural Science Foundation of China (Grant Nos: 91622115, 91421109, 11574133, 11274003 and 21571097), the Natural Science Foundation of Jiangsu Province (Grant BK20160659), the PAPD project, and the Fundamental Research Funds for the Central Universities.

Author contributions: F. S., Y. S., B. W. and G. W. designed the experiments and supervised the efforts. T. W. grew the CVD graphene. J. G., F. F. and Z. B. fabricated the graphene devices. J. L. fabricated the EDTA-Dy molecules. J. G., Y. Q., S. Z. and L. S. carried out the transport measurement. Z. S. took the AFM measurement. R. W made the discussion part. All of the authors discussed the results and contributed to the production of the manuscript.

Figures and Tables

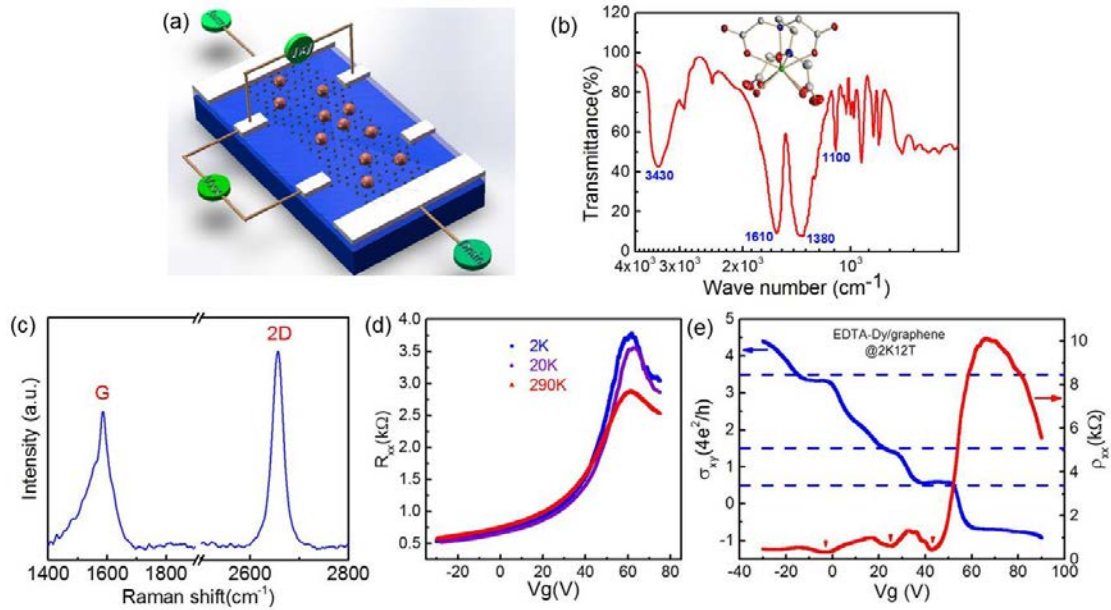


Figure 1. The EDTA-Dy dressed graphene and its device transport. (a) The schematic configuration of the device, where the EDTA-Dy (orange ball) coats the graphene sheet. (b) Infrared spectrum of the EDTA-Dy complex. The inset is the structure of EDTA-Dy, where the green, blue, red and gray balls represent Dy, N, O and C atoms respectively. (c) Raman spectrum of EDTA-Dy dressed graphene, indicating that the sample is a single layer graphene sheet. (d) Resistance as a function of back gate voltage (V_g) for EDTA-Dy dressed graphene at 2, 20 and 290 K. (e) V_g dependence of the longitudinal resistivity ρ_{xx} and the Hall conductivity σ_{xy} measured in a magnetic field of 12 T at a temperature of 2 K, where the Hall conductivity goes quantized and the longitudinal resistivity approaches zero.

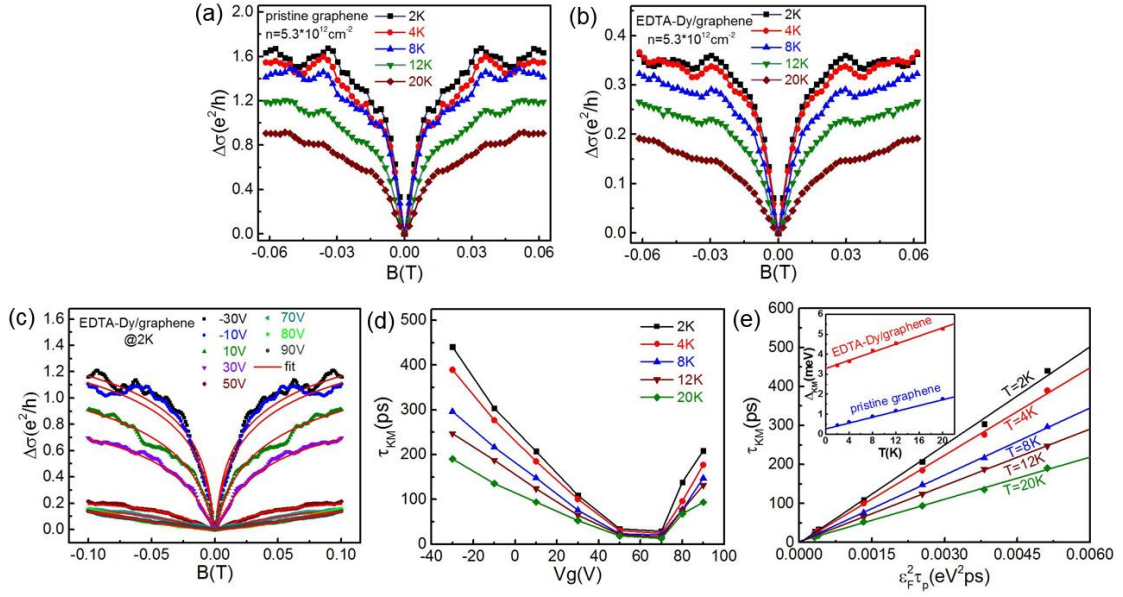


Figure 2. Selectively enhanced KM-type SOI in the graphene device and

Elliot-Yafet plot. (a),(b) The weak localization (WL) of pristine and EDTA-Dy

dressed graphene with the same charge concentration at various temperatures. The

conductance correction is suppressed after the dressing. (c) The WL features of

EDTA-Dy dressed graphene at different V_g while fixing the temperature of 2 K. The

spin scattering time can be extracted from its fitting and the red curves are the fitting

curves. (d) The spin scattering time of EDTA-Dy decorated graphene plotted against

V_g at various temperatures. (e) Fitting between τ_{KM} and τ_p using $\tau_{KM} =$

$\tau_p(\epsilon_F/\Delta_{KM})^2$, resulting in the SOI strength of EDTA-Dy dressed graphene. The inset

is Δ_{D0} of 0.26/3.3 meV for pristine/EDTA-Dy dressed devices, obtained by

extrapolating the temperature to zero.

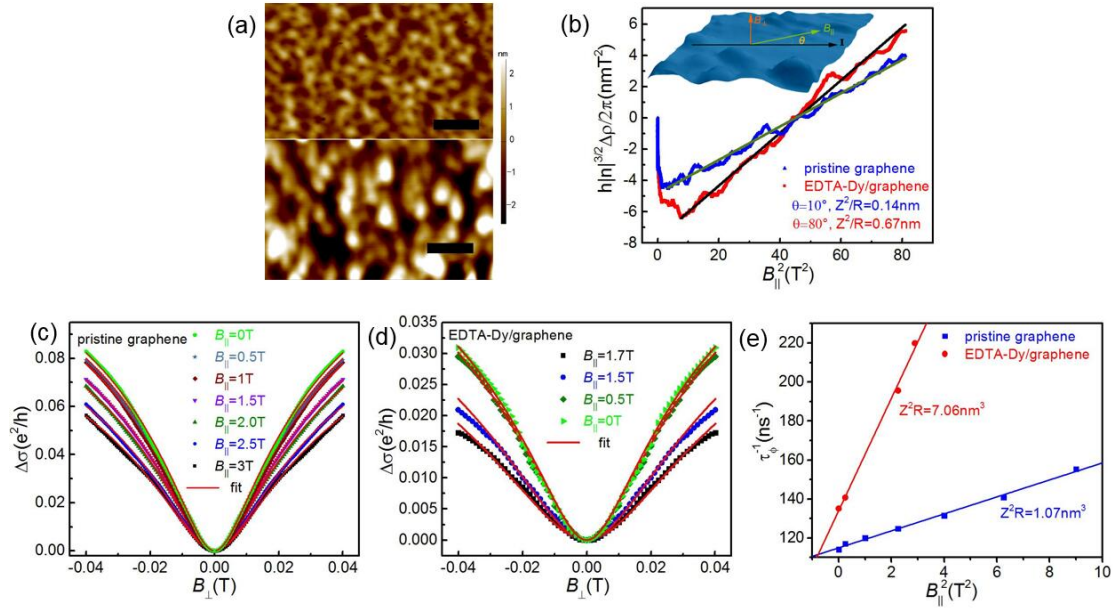


Figure 3. Ripple configuration revealed by the vector magnet measurement. (a) AFM images of pristine graphene (upper) and EDTA-Dy dressed graphene (down). The scale bar is 100 nm. (b) Resistivity of pristine graphene and EDTA-Dy dressed graphene dependent on B_{\parallel}^2 . The solid lines are the fitting according to Eq. (2) using $n=6.44\times 10^{12}\text{ cm}^{-2}$ and $n=4.27\times 10^{12}\text{ cm}^{-2}$. The inset is the measurement configuration. (c),(d) B_{\perp} -dependent magnetoconductivity ($B_{\perp}<0.04\text{ T}$), at a series of fixed B_{\parallel} . Dashed lines are the fitting according to Eq. (3). (c) and (d) correspond to the graphene before and after EDTA-Dy dressing respectively. (e) Extracted values of τ_{ϕ}^{-1} plotted against B_{\parallel}^2 . The dashed lines are the fitting according to Eq. (4).

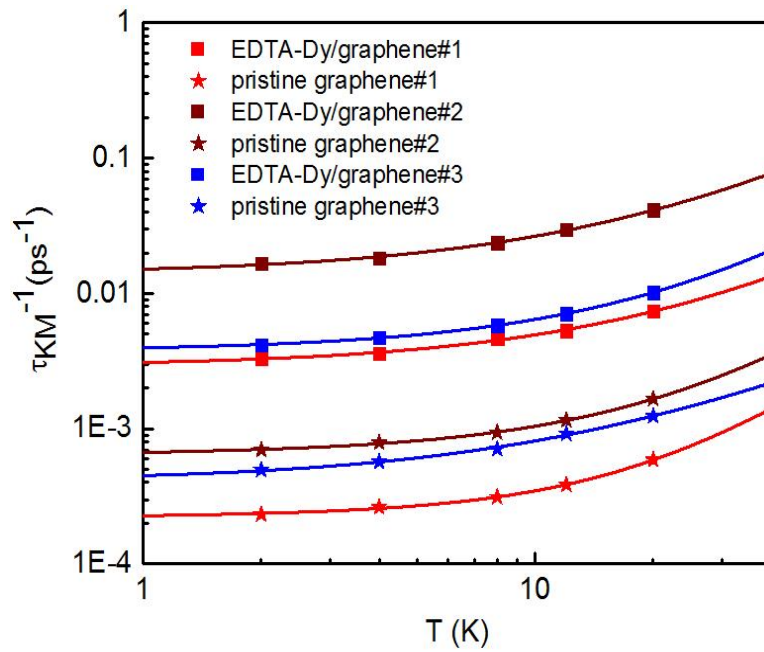


Figure 4. Fitting the spin relaxation by the flexural phonon model. This the data for the spin life time as a function of temperatures. Box and star dots correspond to the graphene devices before and after EDTA-Dy dressing. The solid curves are the fit plot according to the flexural phonon theory.

sample	$n(10^{12}\text{cm}^{-2})$	$\mu(\text{cm}^2\text{V}^{-1}\text{s}^{-1})$	$l_e(\text{nm})$	$D(\text{cm}^2\text{s}^{-1})$	$Z(\text{nm})$	$R(\text{nm})$
#1	10.68/4.28	1919/3226	64.86/71.67	324/358	0.62/1.48	2.7/3.2
#2	9.95/2.73	5342/10160	174.3/415.7	871/2078	N.A.	N.A.
#3	4.01/2.72	3033/6112	168.9/268.3	844/1342	N.A.	N.A.
#4	5.29/3.09	1174/6161	31.52/112.6	158/563	N.A.	N.A.

Table I. Device parameters for four samples before (left) and after EDTA-Dy dressed (right). N.A. means that the value is not measured.